Journal of Alloys and Compounds 519 (2012) 144–148

Contents lists available at SciVerse ScienceDirect

Journal of Alloys and Compounds

journal homepage: www.elsevier.com/locate/jallcom

Magnetic properties of Sm–Fe–Ti nanocomposite magnets with a $ThMn_{12}$ structure

Tetsuji Saito [a,*], Hiroya Miyoshi [a], Daisuke Nishio-Hamane [b]

[a] *Department of Mechanical Science and Engineering, Chiba Institute of Technology, 2-17-1 Tsudanuma, Narashino, Chiba 275-0016, Japan*
[b] *Institute for Solid State Physics, The University of Tokyo, 5-1-5 Kashiwanoha, Kashiwa, Chiba 277-8581, Japan*

ARTICLE INFO

Article history:
Received 9 September 2011
Received in revised form
28 December 2011
Accepted 29 December 2011
Available online 5 January 2012

Keywords:
Rare-earth magnet
Melt-spinning
Nanocomposite magnet
Sm–Fe–Ti alloy

ABSTRACT

Sm–Fe–Ti alloys were produced by melt-spinning followed by heat treatment. The rapidly solidified melt-spun ribbons did not contain any hard magnetic $ThMn_{12}$ phase and thus showed low coercivity. Although no hard magnetic $ThMn_{12}$ phase was obtained by annealing $SmFe_{12}$ melt-spun ribbon, annealed $SmFe_{11.5}Ti_{0.5}$ and $SmFe_{11}Ti$ melt-spun ribbons contained some hard magnetic $ThMn_{12}$ phase and exhibited high coercivity. The highest coercivity of 0.4 MA/m with a remanence of 63.5 A m^2/kg was achieved in the annealed $SmFe_{11}Ti$ melt-spun ribbon with the soft magnetic α-Fe and hard magnetic $ThMn_{12}$ phases. The origin of the high coercivity in the annealed $SmFe_{11}Ti$ melt-spun ribbon was found to be the nanosized grains of the α-Fe and $ThMn_{12}$ phases.

1. Introduction

The search for magnetic materials has extended to the frontiers of physics and material science. With the appearance of high-energy-product Nd–Fe–B permanent magnets, the research and development of permanent magnetic materials has mainly concentrated on alloys containing rare earths [1,2]. One of the achievements of these efforts was the discovery of the RFe_{12} (R: rare-earth) intermetallic compound with a $ThMn_{12}$ structure [3]. The crystal structure of the RFe_{12} compound belongs to the tetragonal space group $I4/mmm$ [4]. The RFe_{12} compound can be obtained with various rare-earth elements, as is the case for other rare-earth compounds such as the $R_2Fe_{14}B$ phase [5]. Since the binary RFe_{12} compound is metastable, the formation of the RFe_{12} phase is rather difficult. However, it was found that the small substitution of T (T = Cr, Mo, V, Ti) for Fe in the RFe_{12} compound resulted in the formation of the $R(Fe,T)_{12}$ compound [6–10]. The Curie temperature and saturation magnetization of the $R(Fe,T)_{12}$ compound depend on the rare-earth metal in a similar manner to the $R_2Fe_{14}B$ phase. Although the $Nd(Fe,T)_{12}$ phase has a high saturation magnetization and a Curie temperature above 500 K, it does not possess c-axis anisotropy, which is essential for permanent magnet materials. On the other hand, the $Sm(Fe,T)_{12}$ phase exhibits c-axis anisotropy because Sm has a Stevens factor αj with a different sign to that of Nd [11] Therefore, studies of the $R(Fe,T)_{12}$ compound have focused on the magnetic properties of the $Sm(Fe,T)_{12}$ phase [12–15].

Only the formation of the $SmFe_{12}$ phase has been reported in sputtered films [16,17], whereas the $Sm(Fe,Ti)_{12}$ phase is usually produced by melt-spinning or mechanical alloying techniques. One of the typical compositions of the $Sm(Fe,Ti)_{12}$ phase that has been extensively studied is the $SmFe_{11}Ti$ phase [9,15]. However, the addition of Ti, which is a nonmagnetic element, reduces the saturation magnetization of the $SmFe_{11}$ phase. It has been reported that the new binary metastable phase of Sm_5Fe_{17} can be directly obtained by annealing Sm–Fe melt-spun ribbon [18]. The $SmFe_{12}$ phase or $Sm(Fe,Ti)_{12}$ phase with lower Ti content may be obtained by annealing Sm–Fe or Sm–Fe–Ti melt-spun ribbons. In this study, $SmFe_{12-x}Ti_x$ (x = 0–1) alloys were produced by the melt-spinning technique. The purpose of this study was to seek the possibility of producing the $SmFe_{12}$ phase or $Sm(Fe,Ti)_{12}$ phase by annealing of the melt-spun ribbons. A systematic investigation of the structures and magnetic properties of these compounds was performed.

2. Experimental

$SmFe_{12-x}Ti_x$ (x = 0–1) alloy ingots were prepared by induction melting of Sm (99.9 wt%), iron (99.9 wt%), and titanium (99.9 wt%) under an argon atmosphere. An alloy ingot of 20 g was induction melted under an argon atmosphere in a quartz crucible having an orifice 0.6 mm in diameter at the bottom. The molten metal was ejected through the orifice with argon onto a chromium-plated copper wheel rotating at a surface velocity of 50 ms^{-1}. The resultant melt-spun ribbons were obtained as fragmented pieces (thickness 10 μm; width 1 mm). In spite of the high oxidation

* Corresponding author. Tel.: +81 47 478 0315; fax: +81 47 478 0329.
E-mail address: tetsuji.saito@it-chiba.ac.jp (T. Saito).

0925-8388/$ – see front matter
doi:10.1016/j.jallcom.2011.12.156

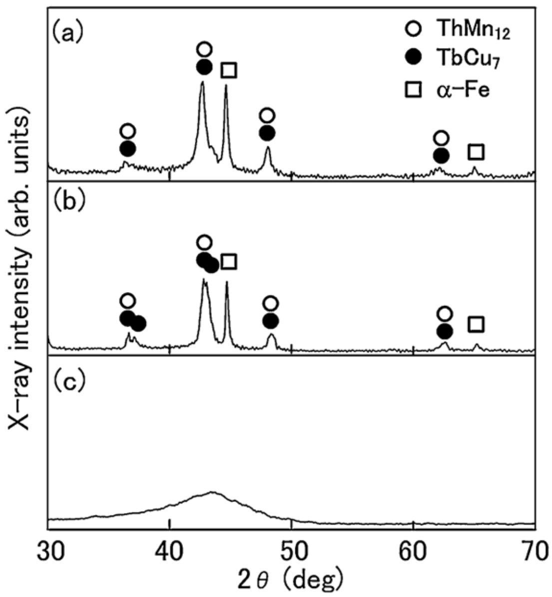

Fig. 1. XRD patterns of the melt-spun ribbons: (a) $SmFe_{12}$, (b) $SmFe_{11.5}Ti_{0.5}$, and (c) $SmFe_{11}Ti$ alloys.

tendency of Sm-containing alloys, the melt-spun ribbons had a smooth metallic surface. The melt-spun ribbons were wrapped with tantalum foil and annealed under an argon atmosphere for 1 h at temperatures between 773 K and 1173 K. The phases in the specimens were examined by X-ray diffraction (XRD) using Cu Kα radiation. The microstructures of the specimens were examined using a transmission electron microscope (TEM) after ion beam thinning. The thermomagnetic curves of the specimens were examined by heating them at a rate of 0.16 K/s in a vacuum using a vibrating sample magnetometer (VSM) with an applied field of 40 kA/m. The VSM was calibrated with a pure nickel sphere. The magnetic properties of the specimens were measured at room temperature by VSM with a maximum applied field of 2 MA/m.

3. Results and discussion

Fig. 1 shows the XRD patterns of the Sm–Fe–Ti melt-spun ribbons. According to the equilibrium phase diagram, the equilibrium phases in the $SmFe_{12}$ alloy at room temperature are the Sm_2Fe_{17} and α-Fe phases. However, no clear diffraction peaks from the Sm_2Fe_{17} phase are observed in the XRD pattern. Due to the high solidification rate of melt-spinning, the metastable phases of the $TbCu_7$ and $ThMn_{12}$ phases were formed in the $SmFe_{12}$ melt-spun ribbon [19,20]. Virtually the same XRD pattern was obtained from the $SmFe_{11.5}Ti_{0.5}$ melt-spun ribbon. This suggests that the $SmFe_{11.5}Ti_{0.5}$ melt-spun ribbon consists of the metastable $TbCu_7$ and $ThMn_{12}$ phases together with the α-Fe phase, as is the case for the $SmFe_{12}$ melt-spun ribbon. Since the diffraction peaks of the $SmFe_{12}$ phase overlap those of the $SmFe_7$ phase, it is difficult to exclude the existence of the $SmFe_7$ phase in the annealed specimen by XRD studies. No clear diffraction peaks, however, are observed in the XRD pattern of the $SmFe_{11}Ti$ melt-spun ribbon. Only a broad halo peak is found, suggesting that the $SmFe_{11}Ti$ melt-spun ribbon is amorphous. It was found that the increase in the Ti content of the Sm–Fe–Ti melt-spun ribbon markedly increased its glass formability.

Fig. 2 shows the thermomagnetic curves of the Sm–Fe–Ti melt-spun ribbons. The thermomagnetic curve of the $SmFe_{12}$ melt-spun ribbon exhibits two magnetic transitions at around 430 K and 1050 K, which correspond to the Curie temperature of the $TbCu_7$ and α-Fe phases, respectively. This suggests that the $SmFe_{12}$ melt-spun ribbon consists of the $TbCu_7$ and α-Fe phases. According to the XRD results, the $SmFe_{12}$ melt-spun ribbon contains the $TbCu_7$, $ThMn_{12}$, and α-Fe phases. However, no trace of the magnetic

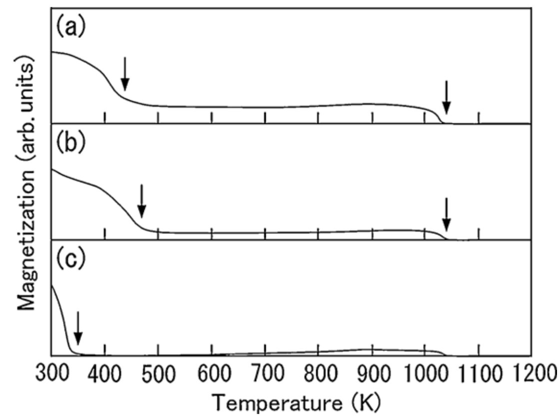

Fig. 2. Thermomagnetic curves of the melt-spun ribbons: (a) $SmFe_{12}$, (b) $SmFe_{11.5}Ti_{0.5}$, and (c) $SmFe_{11}Ti$ alloys.

transition of the $ThMn_{12}$ phase is seen in the thermomagnetic curve. The thermomagnetic curve of the $SmFe_{11.5}Ti_{0.5}$ melt-spun ribbon also exhibits two magnetic transitions at around 470 K and 1050 K, which correspond to the Curie temperature of the $TbCu_7$ and α-Fe phases, respectively. This indicates that the $SmFe_{11.5}Ti_{0.5}$ melt-spun ribbon is composed of the $TbCu_7$ and α-Fe phases. Since the $SmFe_{11.5}Ti_{0.5}$ melt-spun ribbon contains some titanium metal, the observed $TbCu_7$ phase in the $SmFe_{11.5}Ti_{0.5}$ melt-spun ribbon is believed to be the $Sm(Fe,Ti)_7$ phase. Since the solubility of Ti in Fe is very limited, it is considered that the Ti dissolves into the $SmFe_7$ phase and forms the $Sm(Fe,Ti)_7$ phase [21]. The small substitution of Ti for Fe in the $SmFe_{12}$ melt-spun ribbon resulted in an increase in the Curie temperature of the $TbCu_7$ phase. Unlike the case of the $SmFe_{11.5}Ti_{0.5}$ melt-spun ribbon, the thermomagnetic curve of the $SmFe_{11}Ti$ melt-spun ribbon shows one large magnetic transition at around 350 K, indicating that the $SmFe_{11}Ti$ melt-spun ribbon is not composed of the $TbCu_7$ and α-Fe phases. According to the results of the XRD studies, the specimen consisted of the amorphous phase. Thus, the magnetic transition at around 350 K corresponds to the Curie temperature of the amorphous Sm–Fe–Ti alloy with a composition of $SmFe_{11}Ti$.

Fig. 3 shows the hysteresis loops of the Sm–Fe–Ti melt-spun ribbons. Regardless of their Ti content, these melt-spun ribbons showed low coercivity values. This was due to the nonexistence of the hard magnetic $ThMn_{12}$ phase in the melt-spun ribbons. It was therefore essential to obtain the $ThMn_{12}$ phase in order to achieve high coercivity in the melt-spun ribbons. Thus, the Sm–Fe–Ti melt-spun ribbons were annealed at temperatures between 773 K and

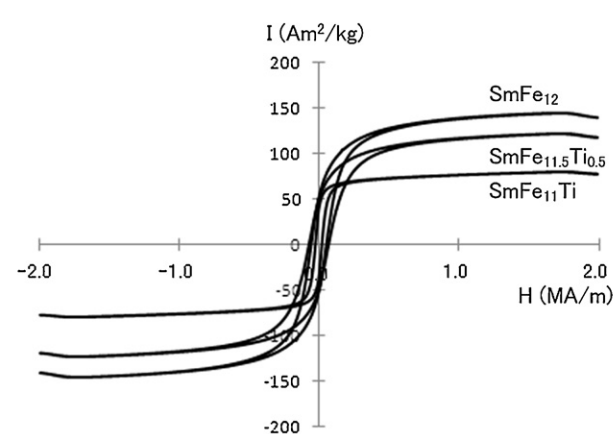

Fig. 3. Hysteresis loops of the $SmFe_{12}$, $SmFe_{11.5}Ti_{0.5}$, and $SmFe_{11}Ti$ melt-spun ribbons.

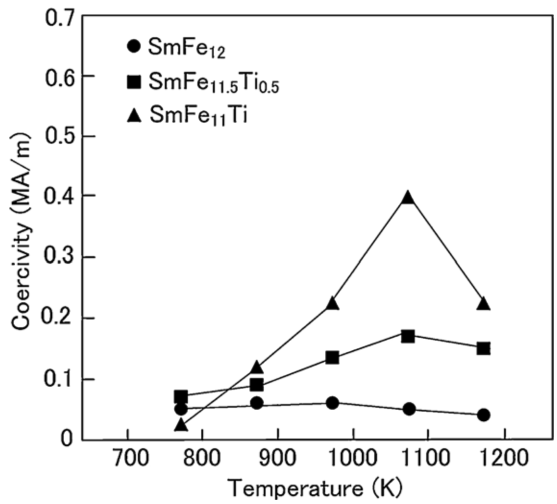

Fig. 4. Dependence of the coercivity of the $SmFe_{12-x}Ti_x$ (x = 0, 0.5, 1) melt-spun ribbon on the annealing temperature.

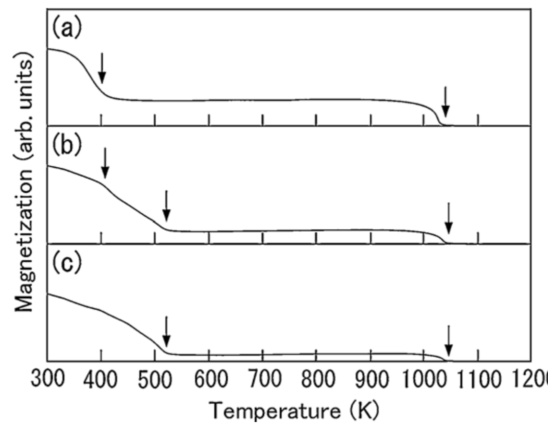

Fig. 6. Thermomagnetic curves of the melt-spun ribbons annealed at 1073 K: (a) $SmFe_{12}$, (b) $SmFe_{11.5}Ti_{0.5}$, and (c) $SmFe_{11}Ti$ alloys.

1173 K for 1 h. Fig. 4 shows the dependence of the coercivity of the $SmFe_{12-x}Ti_x$ (x = 0, 0.5, 1) melt-spun ribbons on the annealing temperature. Although no marked increase in the coercivity value was observed in the $SmFe_{12}$ melt-spun ribbon, the coercivity increased in the $SmFe_{12-x}Ti_x$ (x = 0.5, 1) melt-spun ribbons. The maximum coercivity was achieved in the $SmFe_{11}Ti$ melt-spun ribbon when annealed at 1073 K.

The Sm–Fe–Ti melt-spun ribbons annealed at 1073 K were examined to evaluate differences in their coercivity value. Fig. 5 shows the XRD patterns of the Sm–Fe–Ti melt-spun ribbons annealed at 1073 K. The corresponding thermomagnetic curves are shown in Fig. 6. According to the XRD results, the annealed $SmFe_{12}$ melt-spun ribbon contains the $TbCu_7$, $ThMn_{12}$, and α-Fe phases. However, the thermomagnetic curve of the annealed $SmFe_{12}$ melt-spun ribbon shows two magnetic transitions at around 400 K and 1050 K, which correspond to the Curie temperature of the Sm_2Fe_{17} and α-Fe phases, respectively. This indicates that changes in the magnetic phase can be more effectively determined by thermomagnetic measurements than by XRD studies. Heat treatment of the rapidly quenched $SmFe_{12}$ melt-spun ribbon with the metastable $TbCu_7$ phase does not result in the formation of the $ThMn_{12}$ phase, but in the formation of the equilibrium Sm_2Fe_{17} phase. In contrast, the thermomagnetic curve of the annealed $SmFe_{11.5}Ti_{0.5}$ melt-spun ribbon exhibits three magnetic transitions. The observed magnetic transitions at around 400 K and 1050 K correspond to the Curie temperature of the Sm_2Fe_{17} and α-Fe phases, respectively. The additional magnetic transition at around 520 K is below the reported Curie temperature of the $ThMn_{12}$ phase in the form of a single crystal, but agrees well with the Curie temperature of the $ThMn_{12}$ phase prepared by melt-spinning (527 K) [22,23]. Thus, the magnetic transition at around 520 K is considered to be the Curie temperature of the $ThMn_{12}$ phase. The annealed $SmFe_{11.5}Ti_{0.5}$ melt-spun ribbon contains some $ThMn_{12}$ phase together with the Sm_2Fe_{17} and α-Fe phases. It was found that the metastable $TbCu_7$ phase results in the formation of the $ThMn_{12}$ phase together with the equilibrium Sm_2Fe_{17} phase. On the other hand, the thermomagnetic curve of the annealed $SmFe_{11}Ti$ melt-spun ribbon shows two magnetic transitions. The magnetic transitions at around 520 K and 1050 K correspond to the Curie temperature of the $ThMn_{12}$ and α-Fe phases, respectively. No trace of the magnetic transition of the equilibrium Sm_2Fe_{17} phase is seen in these thermomagnetic curves, indicating that the $SmFe_{11}Ti$ melt-spun ribbon contains two phases: $ThMn_{12}$ and α-Fe. It is known that both the metastable phase and the equilibrium phase can form thermodynamically by annealing of the amorphous

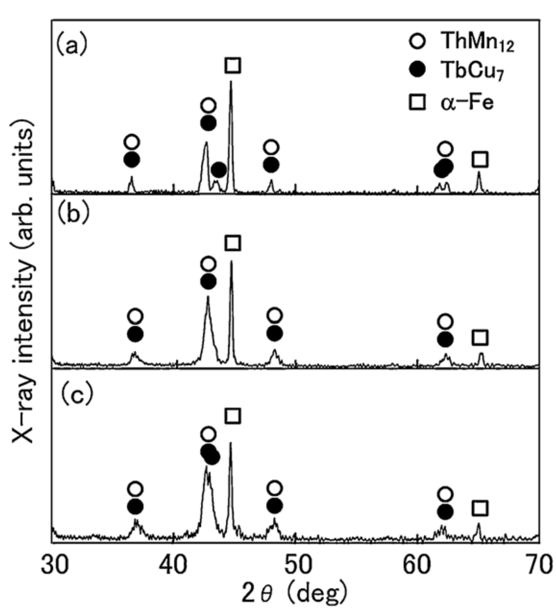

Fig. 5. XRD patterns of the melt-spun ribbons annealed at 1073 K: (a) $SmFe_{12}$, (b) $SmFe_{11.5}Ti_{0.5}$, and (c) $SmFe_{11}Ti$ alloys.

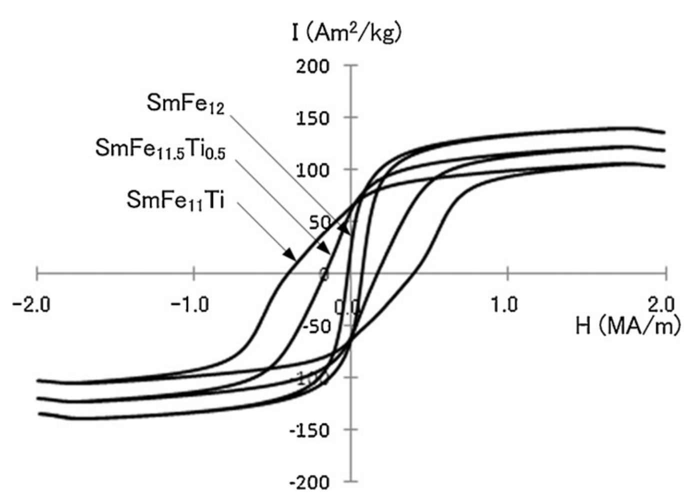

Fig. 7. Hysteresis loops of the $SmFe_{12}$, $SmFe_{11.5}Ti_{0.5}$, and $SmFe_{11}Ti$ melt-spun ribbons annealed at 1073 K for 1 h.

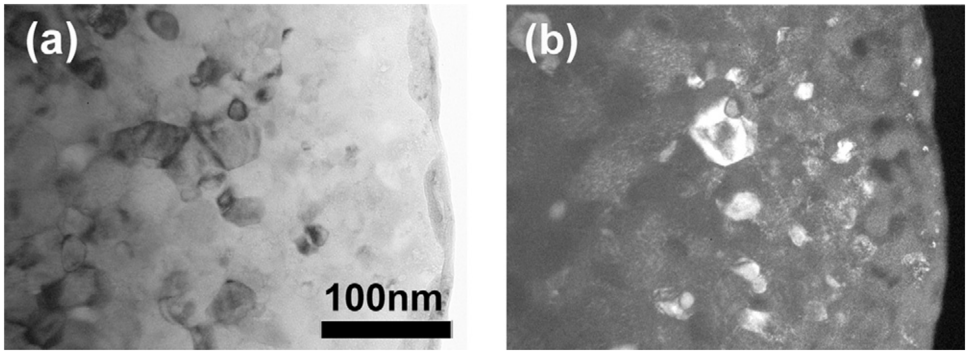

Fig. 8. (a) TEM micrograph and (b) corresponding dark-field image of the $SmFe_{11}Ti$ melt-spun ribbon annealed at 1073 K for 1 h. The white spots in the dark-field image indicate exhibit the existence of Fe particles in the ribbon.

material [24]. Only the $ThMn_{12}$ phase is found in the thermomagnetic curve, suggesting that the formation of the metastable $ThMn_{12}$ phase is kinetically favored over that of the equilibrium Sm_2Fe_{17} phase in this composition when amorphous $SmFe_{11}Ti$ melt-spun ribbon is annealed. Since the α-Fe phase is a soft magnetic phase, the observed high coercivity is due to the formation of the hard magnetic $ThMn_{12}$ phase.

Fig. 7 shows the hysteresis loops of the Sm–Fe–Ti melt-spun ribbons annealed at 1073 K. The annealed $SmFe_{12}$ melt-spun ribbon shows a coercivity value as low as that of the rapidly quenched melt-spun ribbon. This indicates that the formation of the Sm_2Fe_{17} phase in the annealed $SmFe_{12}$ melt-spun ribbon does not result in an increase in coercivity. On the other hand, the annealed $SmFe_{11.5}Ti_{0.5}$ and $SmFe_{11}Ti$ melt-spun ribbons exhibit much higher coercivity than the rapidly quenched melt-spun ribbons. This is due to the formation of the hard magnetic $ThMn_{12}$ phase in the annealed melt-spun ribbons. The annealed $SmFe_{11}Ti$ melt-spun ribbon exhibits a remanence of 63.5 A m^2/kg with a coercivity of 0.4 MA/m.

According to the thermomagnetic studies, the annealed $SmFe_{11}Ti$ melt-spun ribbon consists of the hard magnetic $ThMn_{12}$ phase together with the soft magnetic α-Fe phase. It is known that the existence of the soft magnetic phase in magnets degrades their hard magnetic properties [25]. The presence of the soft magnetic phase in a hard magnetic material usually gives rise to a kink in the hysteresis loop, which is not desirable in hard magnetic materials. Only when the exchange coupling between the soft magnetic phase and hard magnetic phase is dominant in a nanocomposite magnet does the magnet have a smooth hysteresis curve with high coercivity, which are essential properties for a permanent magnet. Thus, the annealed $SmFe_{11}Ti$ melt-spun ribbon with a smooth hysteresis curve is confirmed to be a nanocomposite magnet.

Detailed microstructural studies were carried out to examine the actual grain size of the annealed $SmFe_{11}Ti$ melt-spun ribbon. Fig. 8 shows a TEM micrograph and corresponding dark-field image of the annealed $SmFe_{11}Ti$ melt-spun ribbon. The TEM micrograph shows spherical fine grains of around 10–20 nm in size embedded in faceted grains of around 30–60 nm. The dark-field image revealed that the spherical fine grains were the α-Fe phase. The above results confirm that the annealed $SmFe_{11}Ti$ melt-spun ribbon is a nanocomposite magnet in which the soft magnetic α-Fe phase with grains of around 10–20 nm is embedded in the hard magnetic $ThMn_{12}$ phase with grains of around 30–60 nm. Since it has been found that the annealed $SmFe_{11}Ti$ melt-spun ribbon is a nanocomposite magnet in which the soft magnetic phase is magnetically coupled with the hard magnetic phase and can thus exhibit coercivity, further improvement of the magnetic properties can be expected by optimization of the grain sizes and amounts of these magnetic phases.

4. Conclusion

The structures and magnetic properties of $SmFe_{12-x}Ti_x$ (x = 0–1) melt-spun ribbons were studied. The $SmFe_{12}$ and $SmFe_{11.5}Ti_{0.5}$ melt-spun ribbons consisted of the metastable $TbCu_7$ and α-Fe phases, whereas the $SmFe_{11}Ti$ melt-spun ribbon was amorphous. Regardless of the Ti content of the Sm–Fe–Ti melt-spun ribbons, they showed low coercivity. Heat treatment of the $SmFe_{12}$ melt-spun ribbon resulted in the formation of the equilibrium Sm_2Fe_{17} and α-Fe phases. The resultant annealed melt-spun ribbons showed low coercivity. On the other hand, annealing of the $SmFe_{11.5}Ti_{0.5}$ and $SmFe_{11}Ti$ melt-spun ribbons resulted in an increase in the coercivity. TEM studies revealed that the annealed $SmFe_{11}Ti$ melt-spun ribbon was a nanocomposite magnet in which an extremely fine soft magnetic α-Fe phase with grains of around 10–20 nm in size were embedded in the hard magnetic $ThMn_{12}$ phase with grains of around 30–60 nm, and thus exhibited coercivity.

Acknowledgements

This study was supported by a grant as a Strategic Research Foundation Grant-Aided Project for Private Universities designated by the Ministry of Education, Culture, Sports, Science, and Technology (MEXT), Japan. This work was partly supported by a research grant from The Mazda Foundation. The use of the facilities of the Materials Design and Characterization Laboratory at the Institute for Solid State Physics, The University of Tokyo, is gratefully acknowledged.

References

[1] J.M. Cadogan, H.S. Li, R.L. Davis, A. Margarian, S.J. Collocott, J.B. Dunlop, P.B. Gwan, J. Appl. Phys. 75 (1994) 7114.
[2] F.J.G. Landgraf, F.P. Missell, H.R. Rechenberg, V. Villas-Boas, J.M. Moreau, L. Paccard, J.P. Nozieres, J. Appl. Phys. 70 (1991) 6125.
[3] F.R. de. Boer, H. Ying-kai, D.B. de. Mooij, K.H.J. Buschow, J. Less-Common Met. 135 (1987) 199.
[4] N.C. Liu, N. Kamprath, L. Wickramasekara, F.J. Cadieu, H.H. Stadelmaier, J. Appl. Phys. 63 (1988) 3589.
[5] J.F. Herbst, Rev. Mod. Phys. 63 (1991) 819.
[6] L.X. Liao, Z. Altounian, D.H. Ryan, J. Appl. Phys. 70 (1991) 6006.
[7] L. Shultz, J. Wecker, J. Appl. Phys. 64 (1988) 5711.
[8] Y. Wang, G.C. Hadjipanayis, A. Kim, N.C. Liu, D.J. Sellmyer, J. Appl. Phys. 67 (1990) 4954.
[9] Y. Otani, H.S. Li, J.M.D. Coey, IEEE Trans. Magn. 26 (1990) 2658.
[10] J. Yang, P. Oleinek, K.-H. Müller, J. Appl. Phys. 88 (2000) 988.
[11] E. Tomey, M. Bacmann, D. Fruchart, J.L. Soubeyroux, D. Gignoux, J. Alloys Compd. 231 (1995) 195.
[12] C. Nan-xian, H. Shi-qiang, W. Yu, S. Jiang, J. Magn. Magn. Mater. 233 (2001) 169.
[13] M. Katter, J. Wecker, L. Shultz, R. Grössinger, Appl. Phys. Lett. 56 (1990) 1377.
[14] J. Wecker, M. Katter, K. Schnitzke, L. Shultz, J. Appl. Phys. 67 (1990) 4951.
[15] Q.F. Xiao, X.K. Sun, D.Y. Geng, L. Wei, Z.D. Zhang, Y.C. Chung, J. Magn. Magn. Mater. 140–144 (1995) 1093.

[16] F.J. Cadieu, H. Hegde, A. Navarathna, R. Rani, K. Chen, Appl. Phys. Lett. 59 (1991) 875.
[17] D. Wang, S.H. Liou, P. He, D.J. Sellmyer, G.C. Hadjipanayis, Y. Zhang, J. Magn. Magn. Mater. 124 (1993) 62.
[18] T. Saito, J. Alloys Compd. 440 (2007) 315.
[19] Y. Xingbo, T. Izumi, T. Miyazaki, C. Horie, M. Takahashi, J. Magn. Magn. Mater. 67 (1987) 365.
[20] J.E. Shield, J. Alloys Compd. 291 (1999) 222.
[21] Q.F. Xiao, X.K. Sun, D.Y. Geng, L. Wei, Z.D. Zhang, Y.C. Chuang, J. Magn. Magn. Mater. 1093 (1995) 140–144.
[22] K. Ohashi, Y. Tawara, R. Osugi, M. Shimao, J. Appl. Phys. 64 (1988) 5714.
[23] E.W. Singleton, J. Streszewski, G.C. Hadjipanayis, J. Appl. Phys. 64 (1988) 5717.
[24] K.N. Ishihara, M. Maeda, P.H. Shingu, Acta Metall. 33 (1985) 2113.
[25] Y. Hirose, H. Hasegawa, S. Sasaki, in: L. Schultz, K.-H. Müller (Eds.), Proceedings of the Fifteenth International Workshop on Rare-Earth Magnets and their Applications, Werkstoff-Informationsgesellschaft mbH, Frankfurt, 1998, p. 77.